***Supporting Information***

# Evaluating Fe-MOF/Graphene Nanocomposites for Non-Enzymatic Electrochemical Sensing of Acetaminophen

***Jithin Rafi[a], Thangavelu Kokulnathan[b], Tzyy-Jiann Wang[b*], Murugan Velmurugan[c], Bernaurdshaw Neppolian[a*]***

*[a]Energy and Environmental Remediation Lab, Department of Chemistry, Faculty of Engineering and Technology, SRM Institute of Science and Technology, Kattankulathur, Chengalpattu 603 203, Tamil Nadu, India.*

*[b]Department of Electro-Optical Engineering, National Taipei University of Technology, Taipei 10608, Taiwan.*

*[b]Department of Chemistry, K. Ramakrishnan College of Technology, Samayapuram, Tiruchirappalli 621 112, Tamil Nadu, India.*

*Corresponding Authors:

f10939@ntut.edu.tw (T. J. Wang)

neppolib@srmist.edu.in (B. Neppolian)

## Materials

Anhydrous iron chloride ($FeCl_3$), 2-amino terephthalic acid ($NH_2$-BDC), and acetaminophen (APAP) were purchased from Sigma Aldrich. Dimethylformamide (DMF) was purchased from SRL Chemicals Ltd. while graphene (GR; 8 nm) was acquired from Uni Region Biotech, Taiwan. All chemicals and reagents used in this study were of analytical grade. Deionized (DI) water was used for all electrochemical studies, and a 0.05 M phosphate buffer solution (PBS) served as the supporting electrolyte.

## Instrumentation

X-ray diffraction (XRD) patterns were recorded using a BRUKER X-ray diffractometer with Cu Kα radiation (λ = 1.5418 Å). Fourier-transform infrared (FTIR) spectra were obtained using a PerkinElmer Frontier FTIR spectrometer. Raman spectra were acquired using a Horiba Scientific Raman spectrometer with a 532 nm excitation laser. The zeta potential of the prepared materials was measured using a Malvern PANalytical zeta potential analyzer. X-ray photoelectron spectroscopy (XPS) measurement was carried out using a JEOL JPS-9030 spectrometer. Morphological characterization was performed using a field-emission scanning electron microscope (FESEM, JEOL JSM-7800F Prime) equipped with energy-dispersive X-ray (EDX) spectroscopy and elemental mapping capabilities. Transmission electron microscopy (TEM), high-resolution TEM (HRTEM), and selected area electron diffraction (SAED) were carried out using a JEOL-JEM-2100 Plus TEM microscope. Surface area and porosity measurements were conducted by Brunauer–Emmett–Teller (BET) analysis using the nitrogen adsorption–desorption isotherms measured on a Quantachrome Autosorb iQ Station 1 analyzer. APAP determination was performed using reversed-phase HPLC equipped with a C18 column (e.g., Supelco L1, 5 μm). The mobile phase consisted of acetonitrile–water or methanol–water mixtures (pH 3.0–4.0), and the used samples were pretreated by solid-phase extraction using Oasis WAX cartridges. Detection was carried out using a UV detector (243–280 nm) with the retention time of 0.5–3 min, the flow rate of 1.0–1.5 mL $min^{-1}$, and the total run time of 2–10 min. Electrochemical studies were performed on the electrochemical workstations (CHI 1211C & CHI 6273e) employing a three-electrode system, which consists of a glassy carbon electrode (GCE, 3 mm) as the working electrode, an Ag/AgCl (saturated KCl) electrode as the reference electrode, and a platinum wire as the counter electrode. Cyclic voltammetry (CV) measurement was conducted over the potential window of 0–0.8 V. Differential pulse voltammetry (DPV) measurement was performed with the pulse amplitude

of 0.05 V, the pulse width of 0.05 s, the pulse period of 0.5 s, and the potential range of 0–0.8 V.

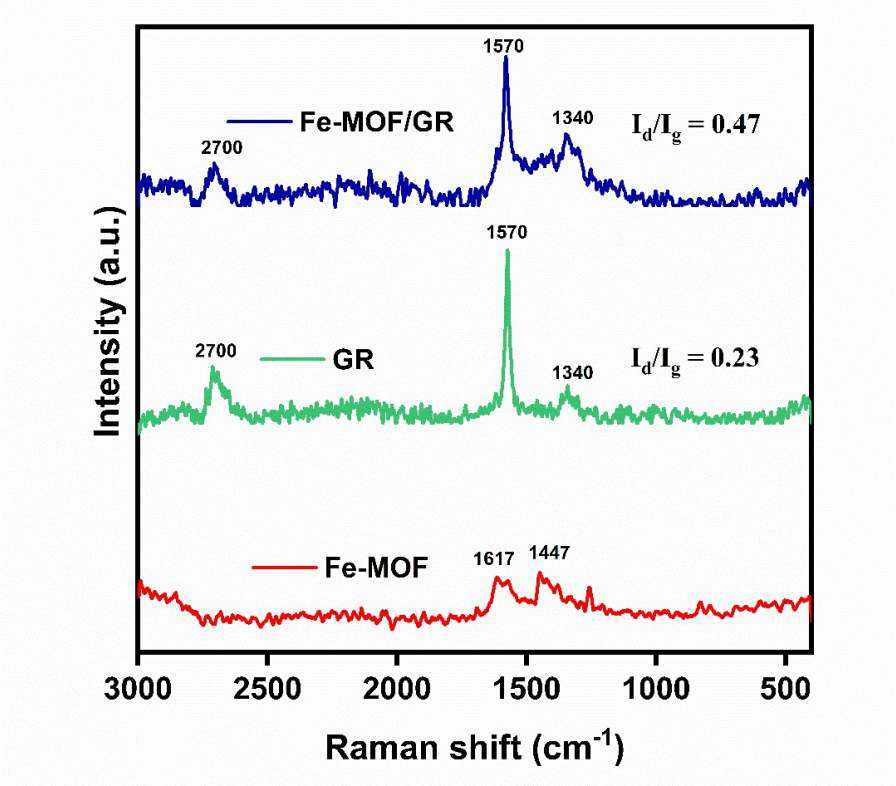


**Fig. S1** Raman spectra of Fe-MOF, GR and Fe-MOF/GR nanocomposite.

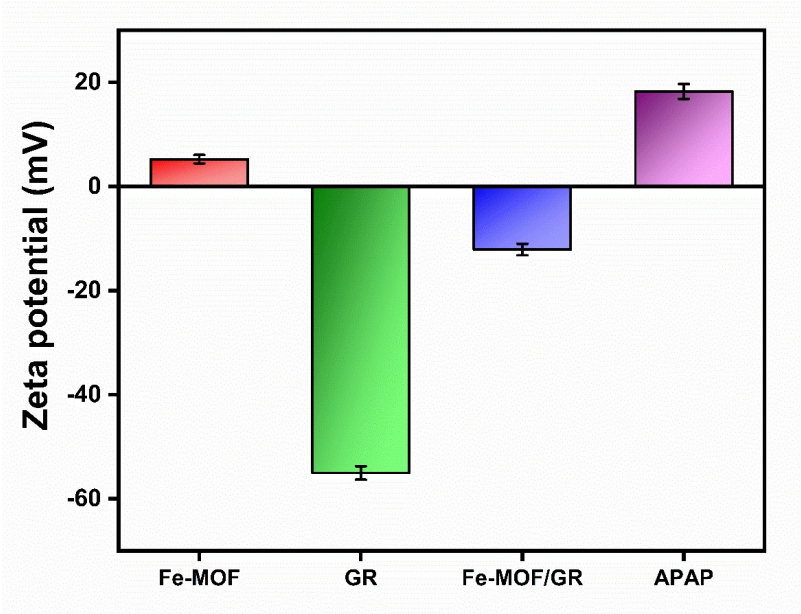


**Fig. S2** Zeta potential values for Fe-MOF, GR, Fe-MOF/GR nanocomposite and APAP.

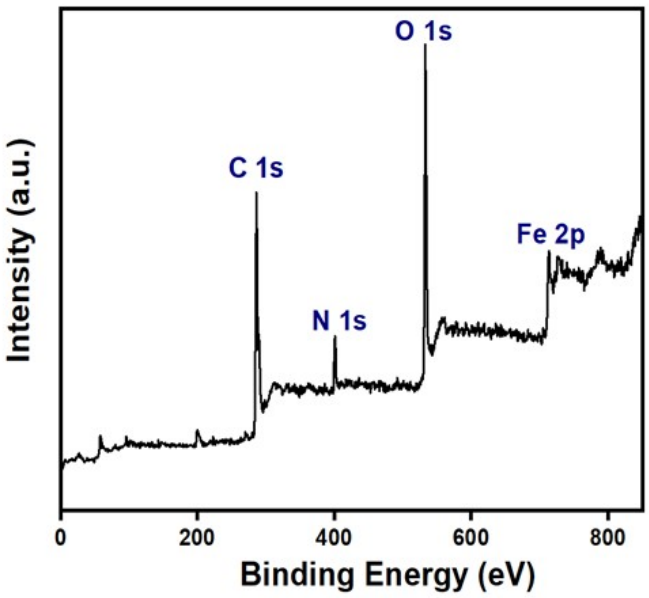


**Fig. S3** XPS survey spectrum of Fe-MOF/GR nanocomposite.

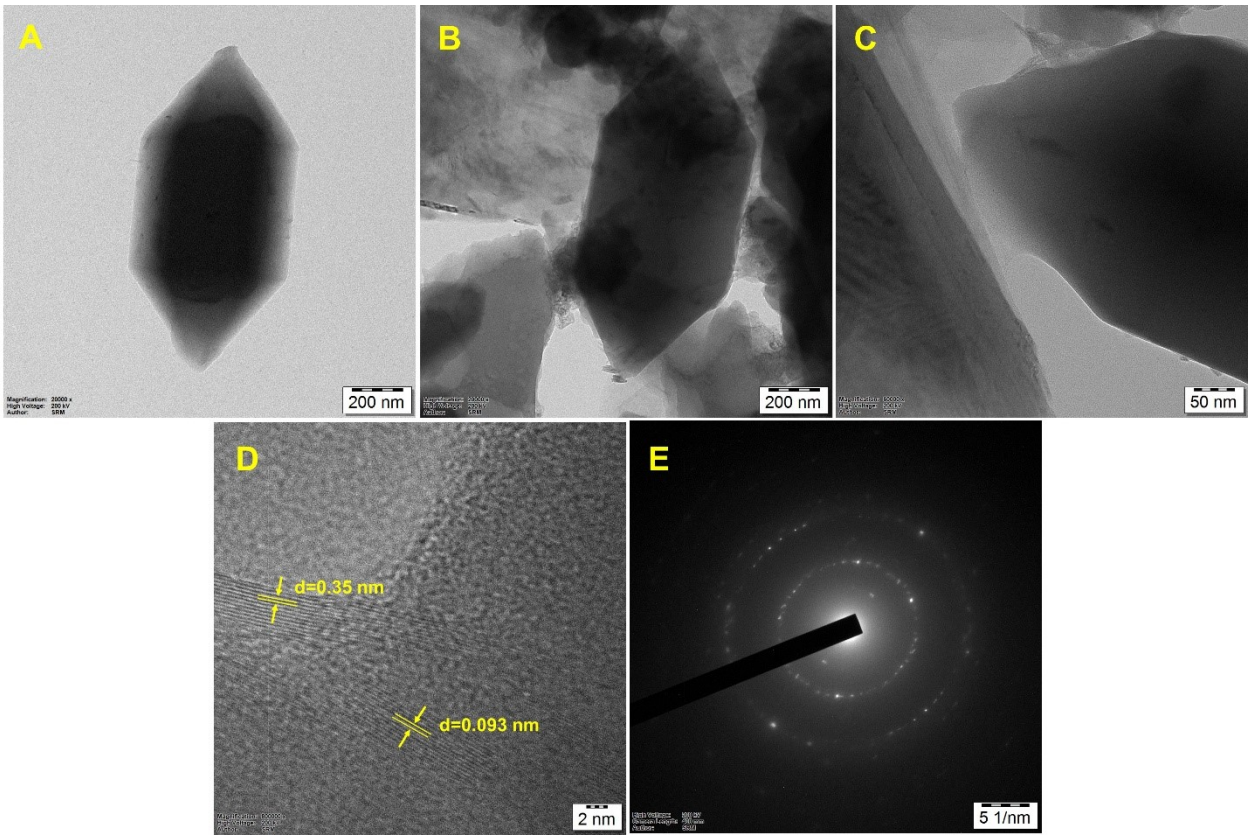


**Fig. S4** TEM images of (A) Fe-MOF and (B, C) Fe-MOF/GR nanocomposite; (D) HRTEM image and (E) SAED pattern of the Fe-MOF/GR nanocomposite.

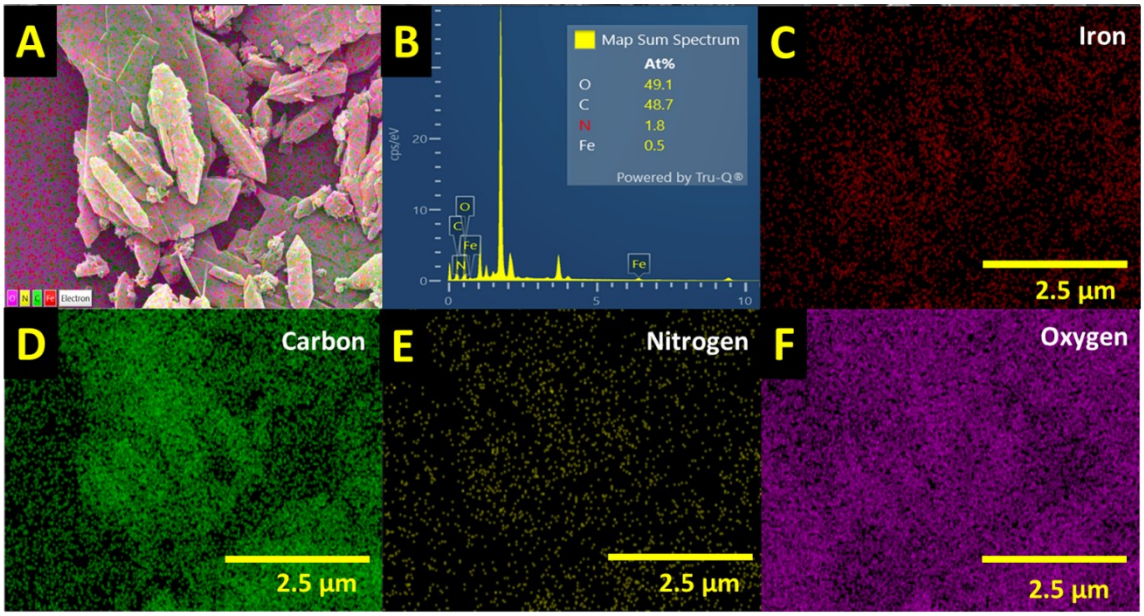


**Fig. S5** (A) Combined color-coded elemental mapping image, (B) EDX spectrum, and elemental mapping images of the Fe-MOF/GR nanocomposite for (C) Fe, (D) C, (E) N, and (F) O elements.

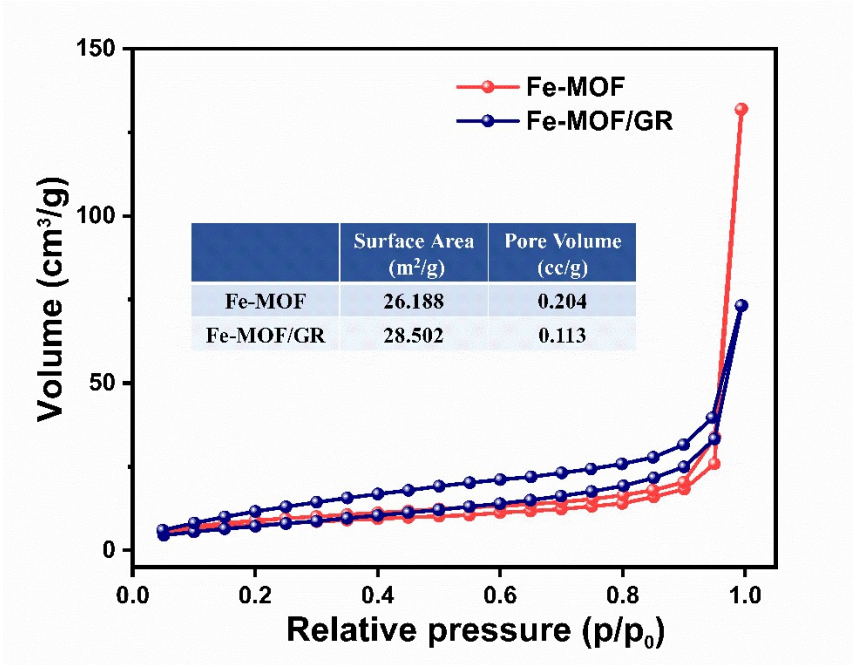


**Fig. S6** $N_2$ adsorption–desorption isotherms of Fe-MOF and Fe-MOF/GR nanocomposite.

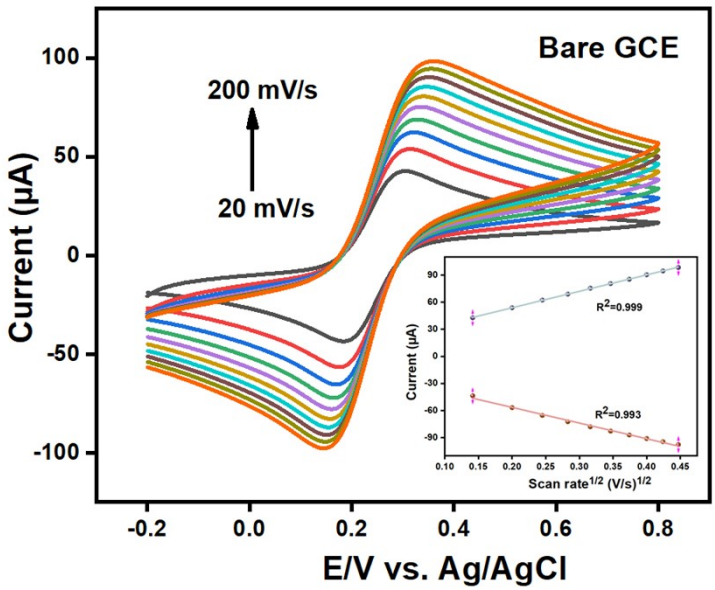


**Fig. S7** CV curves of bare GCE using 5 mM $[Fe(CN)_6]^{3-/4-}$ containing 0.1 M KCl solution at different scan rates (Inset: Plots of the peak redox current versus the square root of the scan rate).

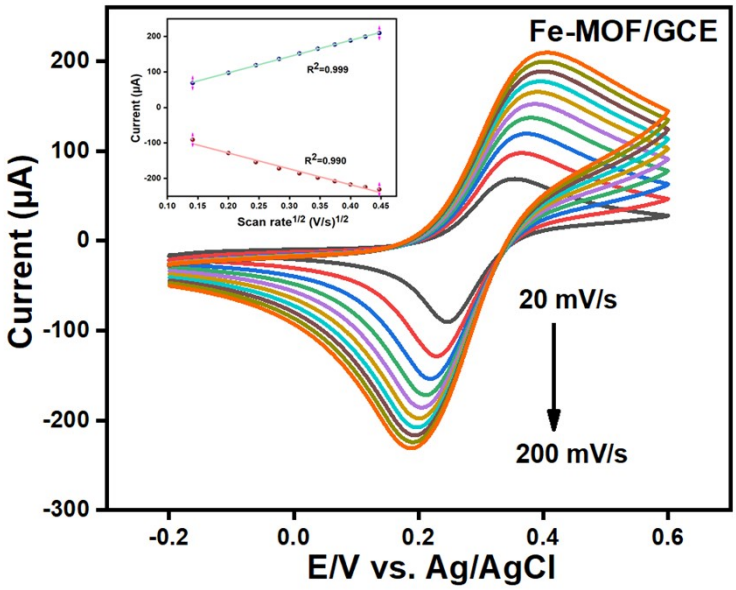


**Fig. S8** CV curves of Fe-MOF/GCE using 5 mM $[Fe(CN)_6]^{3-/4-}$ containing 0.1 M KCl solution at different scan rates (Inset: Plots of the peak redox current versus the square root of the scan rate).

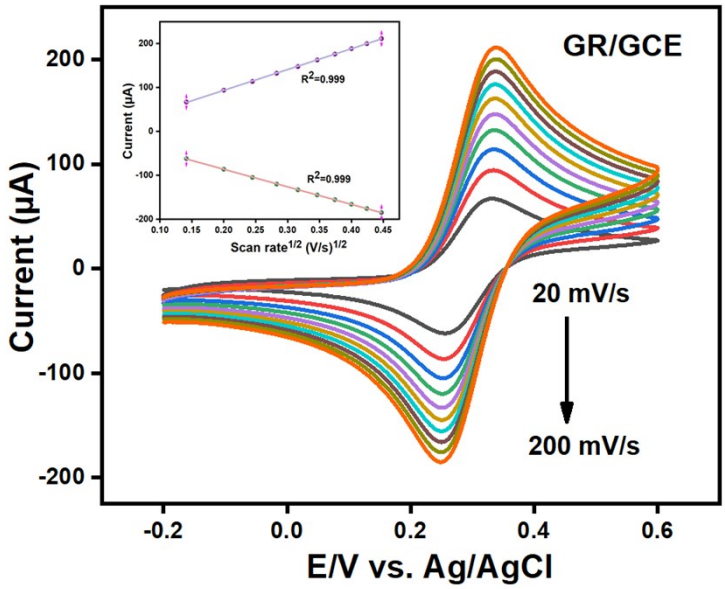


**Fig. S9** CV curves of GR/GCE using 5 mM $[Fe(CN)_6]^{3-/4-}$ containing 0.1 M KCl solution at different scan rates (Inset: Plots of the peak redox current versus the square root of the scan rate).

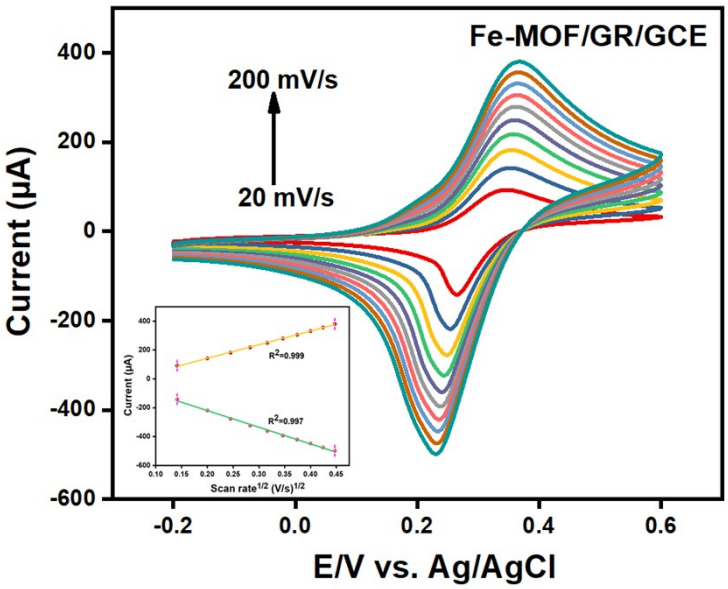


**Fig. S10** CV curves of Fe-MOF/GR/GCE using 5 mM $[Fe(CN)_6]^{3-/4-}$ containing 0.1 M KCl solution at different scan rates (Inset: Plots of the peak redox current versus the square root of the scan rate).

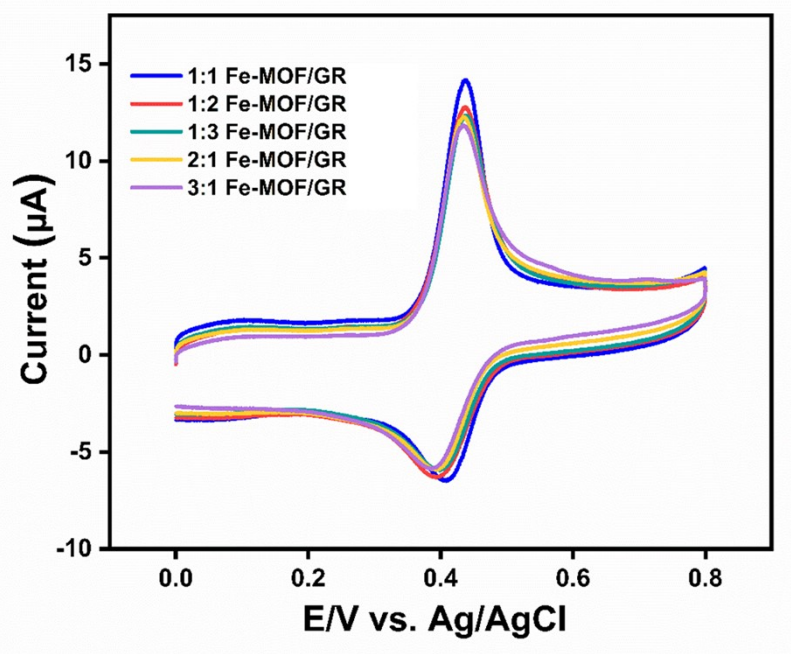


**Fig. S11** CV curves of different ratios of Fe-MOF/GR composite in the presence of 150 μM APAP.

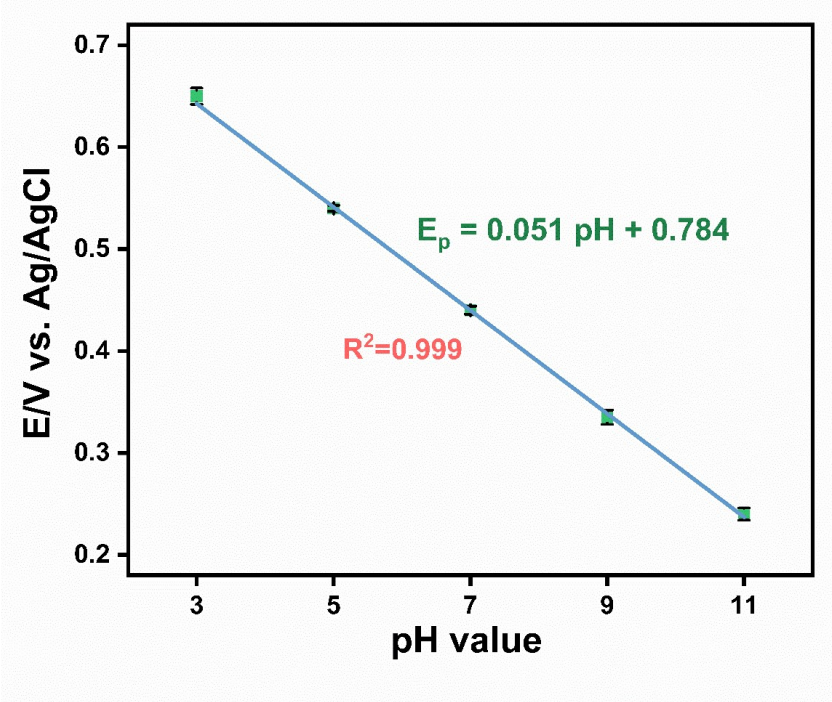


**Fig. S12** Relation between the peak oxidation potential and the pH value for APAP detection.

**Table S1** Recovery comparison of APAP detection in real samples using the standard HPLC method and the electrochemical method using the Fe-MOF/GR/GCE.

| Sample | Added concentration (μM) | HPLC Method | | Electrochemical Method | |
|---|---|---|---|---|---|
| | | Found concentration (μM) | Recovery (%) | Found concentration (μM) | Recovery (%) |
| River water | 1.00 | 0.97 | 97.0 | 0.98 | 98.00 |
| | 2.00 | 1.93 | 96.5 | 1.91 | 95.50 |
| | 4.00 | 3.96 | 99.0 | 3.93 | 98.20 |
| Artificial urine | 1.00 | 0.96 | 96.0 | 0.96 | 96.00 |
| | 2.00 | 1.95 | 97.5 | 1.93 | 96.50 |
| | 4.00 | 3.90 | 97.5 | 3.85 | 96.20 |